AIAA JOURNAL
Vol. 30, No. 7, July 1992

Impact Response of Graphite/Epoxy Cylindrical Panels

A. Palazotto* and R. Perry†
Air Force Institute of Technology, Wright-Patterson Air Force Base, Ohio 45433
and
R. Sandhu‡
Wright Laboratory, Wright-Patterson Air Force Base, Ohio 45433

Graphite/epoxy curved cylindrical panels were impacted in the center by an impact machine capable of measuring load during the test. Load, deflection, and strain as functions of time were measured for six symmetric lay-up configurations for impact energies of 0.5–4.5 ft-lb. Damage was produced in all panels for certain impact energies. The extent and location of damage was determined from C-scans and optical microscopy of panel cross sections. The cross sections indicated that both delamination and transverse cracking contribute to internal damage. An in-house nonlinear finite element code was used to predict the panel deflections and stresses. The analysis produced good results in predicting the $[0/90]_{3s}$ panel deflection, and indicated transverse failure stresses were present in the panel center region. The deflections indicated that the panel boundary was between simply supported and clamped conditions, with good agreement obtained for hinged support at each edge.

Introduction

THE use of composite materials in aerospace applications, where high strength-to-weight and stiffness-to-weight ratios are essential, requires the understanding of the laminate behavior not only under in-plane loading, but also its response to forces normal to the laminate, including impact loading.

Characterization of the laminate response under impact loading is particularly important because of the susceptibility of the composite to low-velocity impact damage from tools and other objects dropped during manufacture or repair. Several types of damage can result from impact including delaminations, transverse cracks within the layers, surface damage or indentation, and layer tensile failure.

The purpose of this research was to compare impact damage in cylindrical graphite/epoxy panels to a dynamic analysis of the impact. Using the force-time response measured during the experiment as the applied loading, the experiments were analyzed with a finite element model based on shell elements incorporating transverse shear deformation. Deflection and strain output were then compared to the experimental results. Post-test inspection to quantify the extent and type of damage used both C-scans and optical microscopy of the panel cross sections.

Experimentation

Materials

The specimens used in this series of tests were curved cylindrical panels made of AS4/3501-6 graphite/epoxy. The panels have surface dimensions of 8 × 8 in. with a radius of curvature of 12 in. Six stacking sequences were investigated: $[0/90]_{3s}$, $[90/0]_{3s}$, $[\pm 45]_{3s}$, $[0/90]_{6s}$, $[90/0]_{6s}$, and $[\pm 45]_{6s}$.

Received Feb. 6, 1991; presented as Paper 91-1078 at the AIAA/ASME/ASCE/AHS/ASC 32nd Structures, Structural Dynamics, and Materials Conference, Baltimore, MD, April 8–10, 1991; revision received Oct. 5, 1991; accepted for publication Oct. 21, 1991.

*Professor, Aeronautics and Astronautics Department. Associate Fellow AIAA.
†Graduate Student.
‡Aerospace Engineer, Structural Division. Member AIAA.

Instrumentation

The specimens were held in place between an aluminum support block and a curved steel plate and secured by 12 bolts surrounding the panel edges. The cutout area in the plate and support block measures 5 × 5 in. (see Fig. 1).

The panels were impacted normal to the surface in the panel center by a 6.84-lb drop weight impact machine. A load cell is attached to the drop weight to measure the load applied by the impactor during the time it is in contact with the panel. The impact velocity is determined from the time required for a metal strip to pass a photodetector beam placed above the panel surface.

In addition, a direct measurement of the panel deflection at its center was obtained using the MTI-1000 Fotonic Sensor. This instrument is a displacement sensor equipped with both emitting and collecting optical fibers. This instrument is placed under the panel and aimed at the target center at a point directly opposite the impact location. The emitting fibers send out a beam of light that is focused on a small area of the target. The light is reflected from a piece of reflective tape affixed to the back of the target beneath the impact point and collected by the collecting optics. Based on the distance of the target from the collecting optics, the amount of light collected increases as the target gets closer to the optic probe, as long as the probe is not near the focal length from the target. The light level seen by the collecting fibers is converted by the MTI-1000 to a dc voltage signal, which is collected by a high-speed data acquisition system.

A stacked rosette of strain gauges was attached to the panel underside at a point 0.5 in. along the circumferential direction from the panel center, measuring the 0- (longitudinal), 90- (circumferential), and 45-deg strains.

The IEEE-488 bus to which the strain gauges and displacement transducer signals were sent has a frequency response up to 1 MHz. For these experiments, data were collected at 100 kHz. The MTI-1000 has a low-pass filter response with rolloff occurring above 100 KHz. The response of the strain gauges has been shown to be adequate to measure dynamic events of duration of a few microseconds.[1] The load cell response is limited by the data acquisition equipment to which it is connected, set to collect measurements at 40 kHz.

Experimental Results

The experiments produced measurements of a number of parameters, including load, deflection, strain, and impact

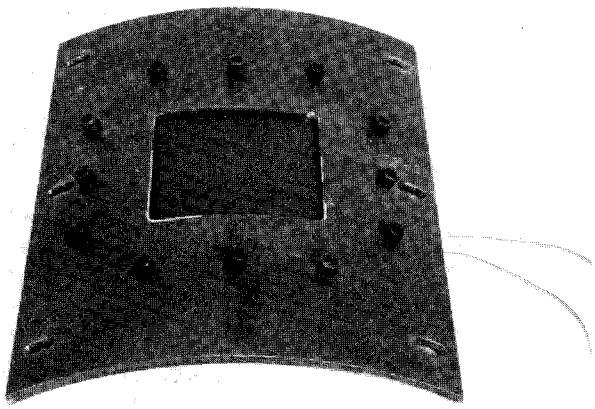

Support Block and Hold-down Plate

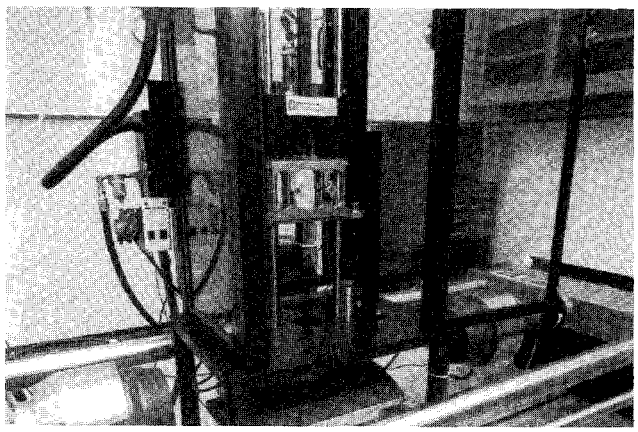

Dynatup Impact Test Machine

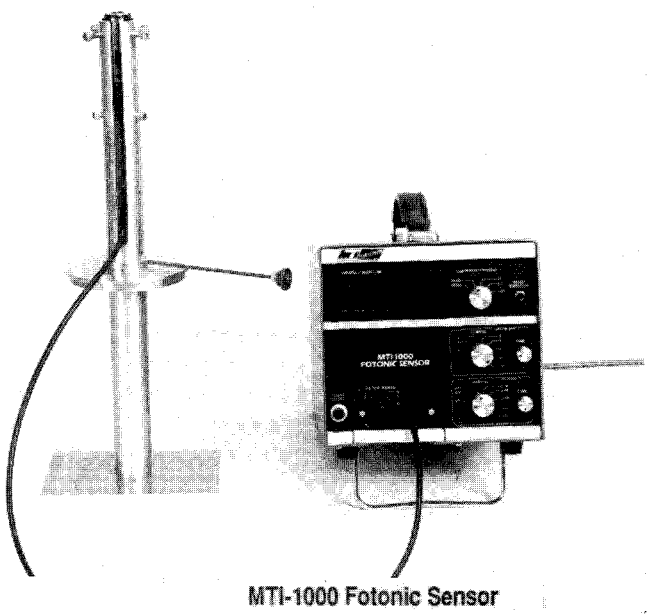

Fig. 1 Test setup.

energy. Figure 2 shows an example plot of load and energy as functions of time. The load shows a large oscillatory behavior beginning as the load reaches a level of about 290 lb; however, the fluctuations subside as the load is removed. In this instance, damage was produced in the panel as confirmed by C-scans and cross sectioning of the panel. By comparison, panels impacted at lower drop heights (and proportionately lower impact energies) did not produce this oscillatory behavior and showed no damage under C-scan,

The time period over which the load is applied has been observed to be constant for any given laminate stacking sequence and thickness. The loading times were 10.4, 9.9, and 11.3 ms for $[0/90]_{3s}$, $[90/0]_{3s}$, and $[\pm 45]_{3s}$, respectively, and 4.6, 4.5, and 4.5 ms for $[0/90]_{6s}$, $[90/0]_{6s}$, and $[\pm 45]_{6s}$, respectively. Consequently, the loading function has been idealized as a sinusoidal force with amplitude directly proportional with the impact velocity. This correlates well with the measured loading function.

The displacement probe and strain gauge responses are shown in Figs. 3 and 4 for two $[0/90]_{3s}$ panels; the first shows the response at low impact energy (no damage produced in the panel) and the second shows the response at a high enough impact energy to cause damage. At the time damage occurs to the panel, the 90-deg (circumferential) strain shows a marked increase, whereas the other two strain measurements show only a small change.

The displacement probe signal rapidly drops at the time of material failure. The cause of this is distortion of the reflective tape applied to the panel. However, the displacement up to this time is measured accurately by the instrument.

The displacements at which damage occur are approximately 0.13 in. for the $[0/90]_{3s}$ and $[\pm 45]_{3s}$ panels, 0.10 in. for the $[90/0]_{3s}$ panel, and 0.07–0.10 in. for the 24-ply lami-

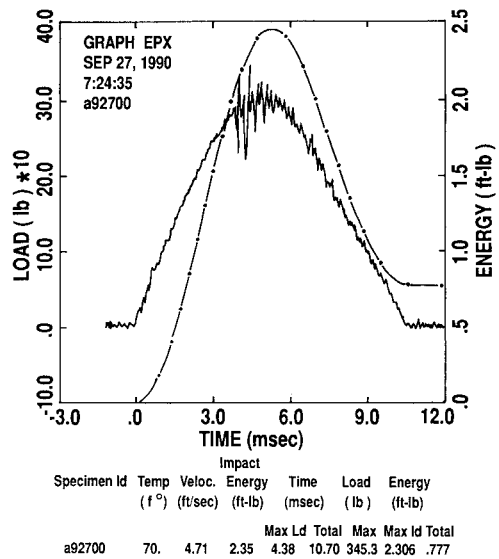

Specimen Id	Temp (f °)	Veloc. (ft/sec)	Impact Energy (ft-lb)	Time (msec)	Load (lb)	Energy (ft-lb)
				Max Ld	Total	Max	Max Id	Total
a92700	70.	4.71	2.35	4.38	10.70	345.3	2.306	.777

Fig. 2 Example of load and energy plot from Dynatup.

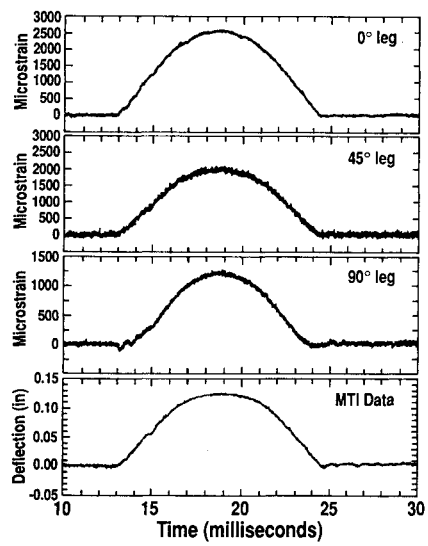

Fig. 3 Strain and deflection for $[0/90]_{3s}$ panel, impact energy = 1.38 ft-lb.

nates. The deflection at which damage initiates in the $[0/90]_{3s}$ and $[\pm 45]_{3s}$ panels is over twice the panel thickness, accentuating the need for a nonlinear analysis.

The panels that sustained damage (as identified by a C-scan) were cross sectioned along the longitudinal axis using a water-cooled diamond saw. The central region was removed from the panel and potted in epoxy. The samples were polished and photographed with an optical microscope.

A photograph of the $[0/90]_{3s}$ specimen cross section is shown in Fig. 5. The panel shows two modes of damage: delamination between the individual layers and transverse cracking within the circumferential (90-deg) layers. The delamination occurs at 90/0 interfaces near the panel center.

Analysis

Approaches to the solution of nonlinear geometric problems incorporating transverse shear deformation without the use of shear correction factors have been investigated by Reddy[2] and Dennis and Palazotto.[3] The static solution derived by Dennis and Palazotto has been incorporated into a dynamic analysis by Tsai and Palazotto.[4] This method has been used in the analysis of the experimental data.

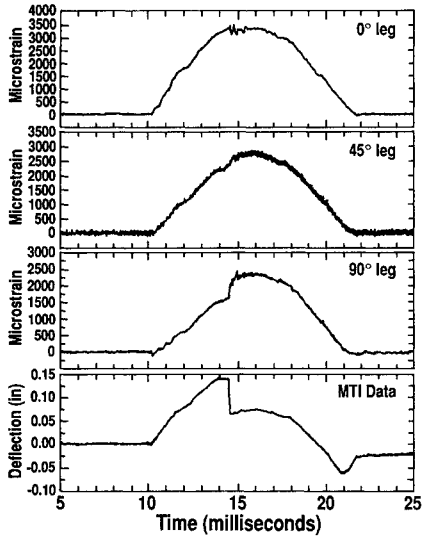

Fig. 4 Strain and deflection for $[0/90]_{3s}$ panel, impact energy = 2.3 ft-lb.

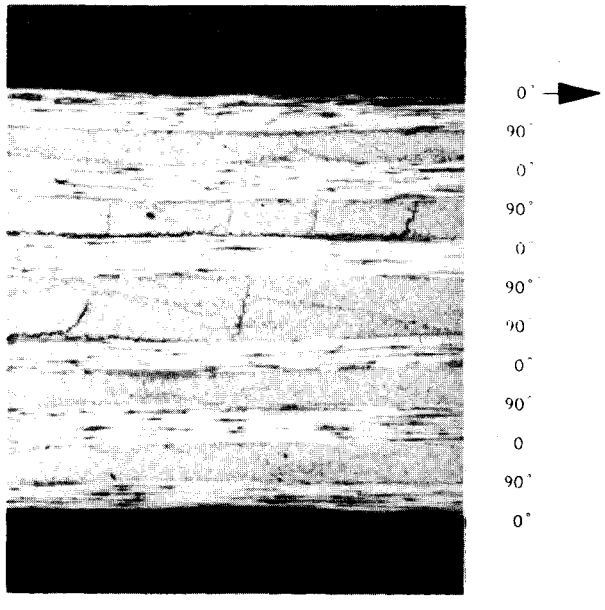

Fig. 5 View of $[0/90]_{3s}$ cross section beneath impact point: 50× magnification.

The Dennis-Palazotto approach assumes a parabolic transverse shear-strain distribution through the thickness, satisfying the requirement that the transverse shear strains be zero at the upper and lower surfaces. The lamina is assumed to be transversely isotropic relative to the 2-3 plane. By neglecting the normal stress σ_{zz} but retaining the τ_{xz} and τ_{yz} terms, the stress-strain relation reduces to

$$\begin{Bmatrix} \sigma_1 \\ \sigma_2 \\ \tau_{23} \\ \tau_{13} \\ \tau_{12} \end{Bmatrix} = \begin{bmatrix} Q_{11} & Q_{12} & 0 & 0 & 0 \\ Q_{12} & Q_{22} & 0 & 0 & 0 \\ 0 & 0 & Q_{44} & 0 & 0 \\ 0 & 0 & 0 & Q_{55} & 0 \\ 0 & 0 & 0 & 0 & Q_{66} \end{bmatrix} \begin{Bmatrix} \epsilon_1 \\ \epsilon_2 \\ \epsilon_4 \\ \epsilon_5 \\ \epsilon_6 \end{Bmatrix} \tag{1}$$

where σ_1, σ_2, and σ_6 are the in-plane longitudinal, tangential, and shear stresses, respectively; $\sigma_4 = \tau_{23}$ and $\sigma_5 = \tau_{13}$ the transverse shear stresses; ϵ_1 and ϵ_2 the in-plane strains in the fiber direction and tangential to the fiber direction, respectively; $\epsilon_4 = \gamma_{23}$ and $\epsilon_5 = \gamma_{13}$ the engineering transverse shear strains ($\gamma_{23} = 2\epsilon_{23}$); and $\epsilon_6 = \gamma_{12}$ the in-plane engineering shear strain. The coefficients of the matrix $[Q]$ are as follows:

$$\begin{aligned} Q_{11} &= E_1/(1 - \nu_{12}\nu_{21}) \\ Q_{12} &= \nu_{21}E_2/(1 - \nu_{12}\nu_{21}) \\ Q_{22} &= E_2/(1 - \nu_{12}\nu_{21}) \\ Q_{44} &= G_{23}, \qquad Q_{55} = G_{13}, \qquad Q_{66} = G_{12} \end{aligned} \tag{2}$$

where E_1, E_2, and ν_{12} are the longitudinal and tangential moduli and the in-plane Poisson's ratio, respectively; $\nu_{21} = \nu_{12}E_2/E_1$; and G_{12}, G_{13}, and G_{23} are the shear moduli in the 1-2, 1-3, and 2-3 planes, respectively.

The strain-displacement relationships used in the analysis are the Donnell cylindrical shell relations at the midplane. The expressions derived by Dennis and Palazotto based on the Donnell approximations are as follows:

$$\epsilon_x = \frac{\partial u}{\partial x} + \zeta\frac{\partial \psi_x}{\partial x} + \zeta^3 k\left(\frac{\partial^2 w}{\partial x^2} + \frac{\partial \psi_x}{\partial x}\right) + \tfrac{1}{2}\frac{\partial^2 w}{\partial x^2}$$

$$\epsilon_s = \frac{\partial v}{\partial s} - \frac{w}{R} + \zeta\left[\frac{\partial \psi_s}{\partial s} - \frac{(\partial v/\partial s)}{R}\right] + \zeta^3 k\left(\frac{\partial \psi_s}{\partial s} + \frac{\partial^2 w}{\partial s^2}\right) + \tfrac{1}{2}\frac{\partial^2 w}{\partial s^2}$$

$$\epsilon_{xs} = \frac{\partial u}{\partial s} + \frac{\partial v}{\partial x} + \zeta\left[\frac{\partial \psi_x}{\partial s} + \frac{\partial \psi_s}{\partial x} - \frac{(\partial v/\partial x)}{R}\right] \tag{3}$$

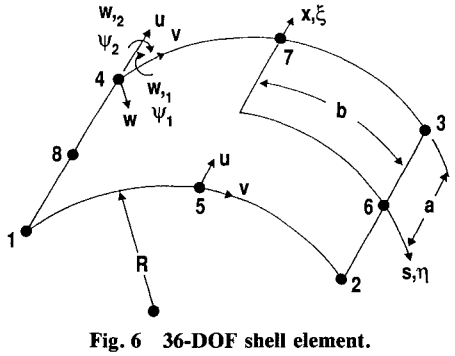

Fig. 6 36-DOF shell element.

$$+ \zeta^3 k\left(2\frac{\partial^2 w}{\partial x \partial s} + \frac{\partial \psi_x}{\partial s} + \frac{\partial \psi_s}{\partial x}\right) + \frac{\partial w}{\partial x}\frac{\partial w}{\partial s}$$

$$\epsilon_{s\zeta} = \left(\frac{\partial w}{\partial s} + \psi_s\right) + 3\zeta^2 k\left(\frac{\partial w}{\partial s} + \psi_s\right)$$

$$\epsilon_{x\zeta} = \left(\frac{\partial w}{\partial x} + \psi_x\right) + 3\zeta^2 k\left(\frac{\partial w}{\partial x} + \psi_x\right)$$

where u, v, and w are the displacements in the x, s, and ζ cylindrical coordinate system, respectively; ψ_x and ψ_s the components of rotation not due to transverse shear deformation; ζ the distance from the midplane measured positive toward the center of curvature; R the radius of curvature; and $k = -4/3h^2$ a thickness parameter.

The finite element formulation is based on the 36-DOF shell element shown in Fig. 6, allowing both rigid-body and shear components of rotation at the corner nodes. The solution algorithm developed by Dennis and Palazotto[3] is applied by Tsai and Palazotto[4] to dynamic problems by the use of Hamilton's principle, such that

$$\delta \int_{t_1}^{t_2} (E - T - W_e)\, dt = 0 \tag{4}$$

where E contains the strain energy, energy loss due to damping, and the body force energy term, T is the kinetic energy, and W_e is the work from external forces. In our analysis, damping and body forces have been neglected.

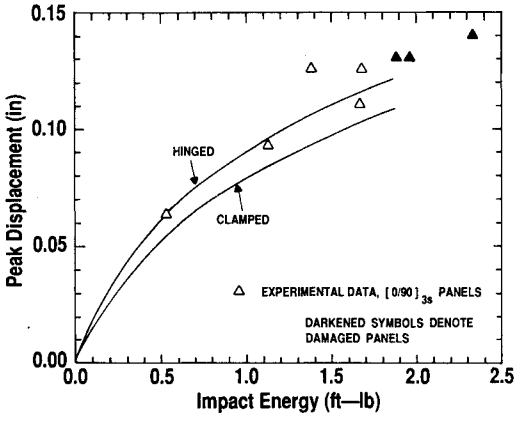

Fig. 7 Experimental and analytical displacements.

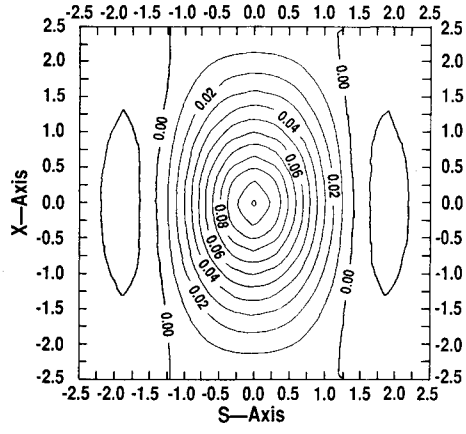

Fig. 8 Radial displacement contours for $[0/90]_{3s}$ panel at failure load of 262 lb.

The finite element formulation obtained from the equations follows the form

$$[M]\{u\} + [C]\{u\} + [K]\{u\} = \{P(t)\} \tag{5}$$

However, the global stiffness matrices incorporate terms up to quadratic in displacement. The stiffness matrix $[K]$ is given by

$$[K] = [K_0 + N_1/2 + N_2/3] \tag{6}$$

where K_0 is an array of constant coefficients, N_1 an array of coefficients that are linear in displacement, N_2 an array of coefficients that are quadratic in displacement, $P(t)$ a column of loads at the nodes, and $\{u\}$ a column of nodal displacements (and rotations).

Force-displacement equilibrium is iteratively solved by the Newton-Raphson method. Newmark integration was used as the time-marching method of integration in all analyses.

Numerical Results

Analysis of several tests were performed to compare the strains and displacements to experimental results.

For the $[0/90]_{3s}$ panels (12 ply), only one quadrant of the test area needed to be modeled since the twisting coefficients A_{16}, A_{26}, D_{16}, and D_{26} are zero for laminates containing only plies with fibers aligned in the 0- and 90-deg directions. An 8×8 grid (0.3125-in. element size) was sufficiently refined for analysis of these tests.

For the $[\pm 45]_{3s}$ test, it was necessary to model the full panel. This is because the bending-twisting coefficients D_{16} and D_{26} are not zero, and so the deflection pattern in the panel will not be symmetric in the four quadrants. The element size was kept constant and the total number of elements was quadrupled to 256.

The time step size used was 0.05 ms in all analyses. Other parameters included in the analysis were the following: mass density $= 1.5088 \times 10^{-4}$ slug/in.^{3}; ply thickness = 0.005 in.; $E_1 = 20.46 \times 10^6$ lbf/in.^{2}; $E_2 = 1.34 \times 10^6$ lbf/in.^{2}; $G_{12} = 0.8638 \times 10^6$ lbf/in.^{2}; $G_{13} = 0.8638 \times 10^6$ lbf/in.^{2}; $G_{23} = 0.4319 \times 10^6$ lbf/in.^{2}; and $\nu_{12} = 0.3131$.

The load was applied as a point force at the panel center. Material outside the 5- × 5-in. opening was neglected. The boundary conditions (BC) are defined as follows:

Clamped:

along $x = 0$ in., symmetry BC: $u = w_{,x} = \psi_x = 0$

along $s = 0$ in., symmetry BC: $v = w_{,s} = \psi_s = 0$

along $x = +2.5$ in.,

geometric BC: $u = v = w = w_{,s} = \psi_s = \psi_x = 0$

along $s = +2.5$ in.,

geometric BC: $u = v = w = \psi_s = w_{,x} = \psi_x = 0$

Hinged:

along $x = 0$ in., symmetry BC: $u = w_{,x} = \psi_x = 0$

along $s = 0$ in., symmetry BC: $v = w_{,s} = \psi_s = 0$

along $x = +2.5$ in.,

geometric BC: $u = v = w = w_{,s} = \psi_s = 0$

along $s = +2.5$ in.,

geometric BC: $u = v = w = w_{,x} = \psi_x = 0$

where subscripts ,x and ,s denote derivatives with respect to x and s, respectively.

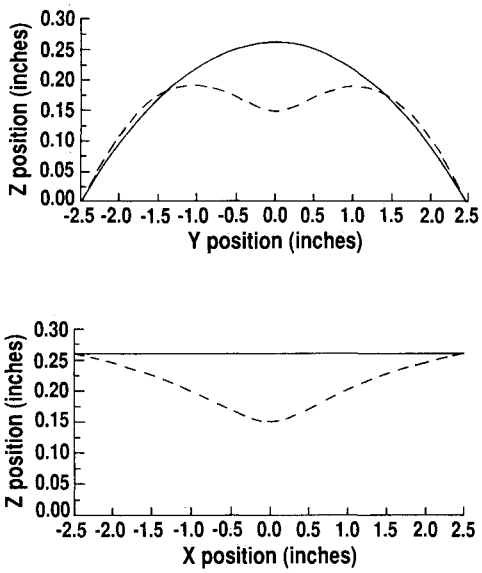

Fig. 9 Deformed geometry of $[0/90]_{3s}$ panel at time of failure.

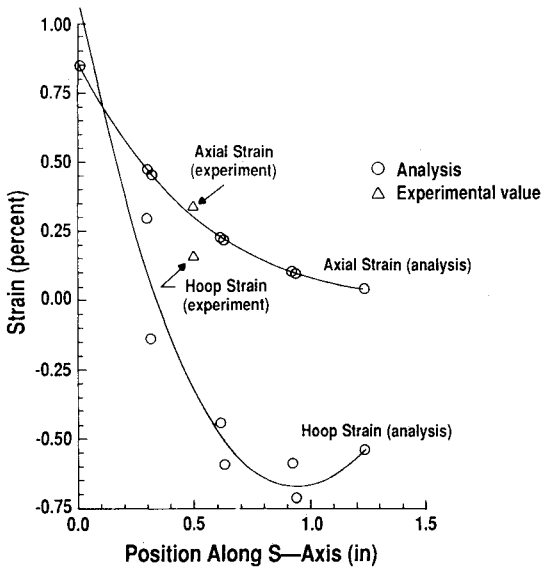

Fig. 10 Comparison of experimental and analytical strains at the time of damage.

Three of the $[0/90]_{3s}$ tests were selected for analysis. The tests were those in which the impactor was dropped 1, 2, and 3.5 in. The corresponding impact energies are 0.55, 1.14, and 1.89 ft-lb, respectively. Damage was produced on the 1.89-ft-lb test, and so this is a good case for comparison. The maximum displacements at the panel center are shown in Table 1 for both clamped and hinged analytical solutions and the experimental measurement from the MTI-1000 Fotonic Sensor.

The results are graphically shown in Fig. 7. At the time that the third panel was damaged, the center deflection was almost exactly half the height from the panel top to its edge. The hinged boundary conditions provide a good comparison with the experimental data. Thus, the hold-down plate may be keeping the panel from pulling out from under it, but the clamping action fails to restrict rotation.

In Fig. 8, the radial displacement contours are shown for the $[0/90]_{3s}$ panel test section at the time of failure, obtained from the analysis. Lines of zero radial displacement are seen to occur at approximately one-fourth of the test section width. Within this area the deflection is inward (positive w), whereas outside the region the displacement is negative in the radial direction. This is more easily visualized in Fig. 9, where the deformed geometry at the time of damage is shown after conversion to Cartesian coordinates.

Comparison of the experimental and analytical strains yields some interesting results. In Fig. 10, the axial and hoop (or longitudinal and circumferential) strains are shown at the time of damage (before the jump in hoop strain) for both the analysis (hinged) and experiment. The analytical results, shown as + symbols, were fit to a third-order polynomial (solid lines). The axial strain in the experiment at the time of damage compares very well with the analysis; however, the hoop strain at the gauge location is significantly different than that predicted by the analysis. The corresponding stresses provide a potential explanation for this phenomena.

The peak tensile stress in the panel occurs on the bottom layer directly beneath the impact point. The maximum tensile stress calculated in the test producing damage is 189 ksi. This is still less than the material ultimate strength, and so no fiber breakage is expected. The experiments showed no surface damage at all on either the bottom or top surface. However, the circumferential (or hoop) stress in the 0-deg layer is approximately 19 ksi at the panel center. This is over twice the material transverse strength, and so transverse failure of the layer is expected. This would be similar to the damage observed in the 90-deg layers from the cross-sectioned specimens. Had the analysis been able to relax the transverse stiffnesses of the elements exceeding the ultimate transverse stress, the surrounding materials would have higher tensile strains and a larger region of the panel underside would have been in tension. The hoop stress drops off rapidly, so that the region over

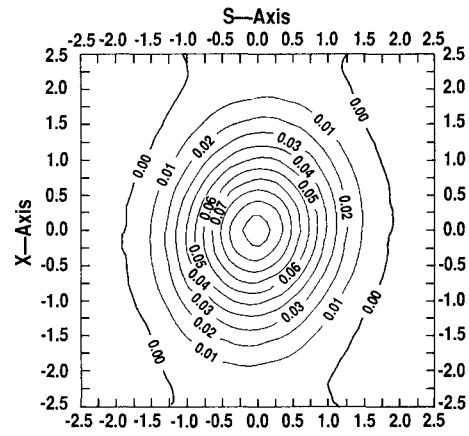

Fig. 11 Radial displacement contours for $[\pm 45]_{3s}$ panel at maximum load.

Table 1 Center deflections of $[0/90]_{3s}$ panel under impact loading

Impact energy, ft-lb	Max load, lb	Peak deflections, in.
0.55	152	0.064 Experimental 0.0645 Analysis hinged 0.0552 Analysis clamped
1.14	216	0.093 Experimental 0.0954 Analysis hinged 0.0836 Analysis clamped
1.89	262[a]	0.131 Experimental 0.1217 Analysis hinged 0.1090 Analysis clamped

[a]Peak load would have been 280 lb if the panel had not been damaged. Deflections reported at time of damage.

Table 2 Center deflection for the $[\pm 45]_{3s}$ panel

Impact energy, ft-lb	Max load, lb	Peak deflection, in.
1.91	265	0.134 Experimental 0.109 Analysis clamped

which damage occurs is predicted to be less than 0.5 in. in diameter. Cross sections and C-scans of the specimen showed that damage occurred on this test over a 0.6-in. diameter.

One $[\pm 45]_{3s}$ panel was analyzed as well. For the ± 45-ply lay up, it is necessary to model the entire panel, since the deflection is not symmetric in the four quadrants. A 16×16 element model was used, with clamped boundary conditions applied on all four edges and the load applied as a point force at the panel center. Results of the analysis are shown in Table 2 for the peak deflection.

A contour map of radial contours is shown in Fig. 11 for this test for the load at the time of damage. It is expected that the hinged boundary conditions would prove more accurate in predicting the peak deflection. Additional analyses should be performed to determine the accuracy of the analysis for other conditions.

Conclusions

Impact damage in graphite/epoxy panels occurs initially from transverse cracking and delaminations. Only at much higher impact energies is it necessary to consider surface damage and fiber failure. The impact energies necessary to produce damage in 12-ply panels can be less than 2 ft-lb. For 24-ply panels, damage occurs in the range of 4–5 ft-lb.

Damage can be characterized by C-scan and optical microscopy of panel cross sections. The C-scans indicate the general shape of the damage, whereas the cross sections identify the layers (or interfaces) in which the damage is present. Damage in the form of transverse cracks is prevalent in all ply lay ups studied. Delaminations occur at interfaces where the directional stiffness changes (by a change in ply angle).

The deflections of the panel were measured using a noncontacting optical sensor. The deflections that correlate with the impact energies necessary to cause damage are approximately 1.5–2 times the thickness of the panel for the 12-ply and 0.8 times the thickness for the 24-ply panels. Strain was also measured on the panel underside using strain gauge rosettes.

A dynamic finite element model incorporating nonlinear geometry and transverse shear deformation predicted the peak deflections of the panel accurately by treating the boundary conditions as hinged. Although clamped boundary conditions were not obtained, the panel edges were restrained from in-plane motion.

The longitudinal strain was predicted accurately by the model; however, the circumferntial (or hoop) strain was underpredicted by a large amount. It is expected that the cause of this discrepancy is reduced transverse stiffness subsequent to the material failure in the transverse layers.

Acknowledgments

This research was carried out under the sponsorship of the Air Force Office of Scientific Research (AFOSR) and with the assistance of the Ohio State University (OSU) Supercomputer Center at Columbus, Ohio. The authors would like to thank AFOSR for the funding and OSU for making available time on the CRAY YMP8/864 supercomputer.

References

[1]Oi, K., "Transient Response of Bonded Strain Gages," *Experimental Mechanics,* Sept. 1966, pp. 463–469.

[2]Reddy, J. N., "Exact Solutions of Moderately Thick Laminated Shells," *Journal of Engineering Mechanics,* Vol. 10, May 1984, pp. 794–809.

[3]Dennis, S. T, and Palazotto, A. N., "Large Displacement and Rotational Formulation for Laminated Shells Including Parabolic Transverse Shear," *International Journal of Nonlinear Mechanics,* Vol. 25, No. 1, 1990, pp. 67–85.

[4]Tsai, C. T., and Palazotto, A. N., "On the Finite Element Analysis of Nonlinear Vibration for Cylindrical Shells," *International Journal of Nonlinear Mechanics,* Vol. 26, No. 14, 1991, pp. 379–388.